J Solid State Electrochem (2012) 16:2061–2069
DOI 10.1007/s10008-011-1608-0

ORIGINAL PAPER

Annealed Ti/Zn-TiO_2 nanocomposites tested as photoanodes for the degradation of Ibuprofen

A. Gomes · T. Frade · K. Lobato · M. E. Melo Jorge · M. I. da Silva Pereira · L. Ciriaco · A. Lopes

Received: 6 September 2011 / Revised: 22 November 2011 / Accepted: 24 November 2011 / Published online: 16 December 2011

Abstract Ti/Zn-TiO_2 electrodes were successfully prepared by the co-deposition method, on a titanium substrate, using an acidic zinc sulphate solution with TiO_2 nanoparticles in suspension. After electrodeposition, samples were heated in air at 450 °C for 6 h. The X-ray diffraction analysis of the deposits point to the metal matrix modification from Zn to ZnO. In addition, the scanning electron microscopy results indicate that the films have a high surface area with a rich morphology, due to the appearance of ZnO needle-shaped grains. The voltammograms recorded, in Na_2SO_4 solution, for these electrodes under illumination at λ=365 nm confirmed the films photoactivity. Photoelectrochemical degradation of Ibuprofen (Ibu) was achieved with the Zn-TiO_2 electrodes after thermal treatment. UV–Vis spectrometry, high-performance liquid chromatography (HPLC), chemical oxygen demand (COD) and total organic carbon (TOC) measurements were performed and data demonstrated that Ibuprofen was efficiently degraded. Absorbance at 220 nm, COD and TOC removals of 35%, 34% and 23%, respectively, were obtained after a 3 h period.

A. Gomes (✉) · T. Frade · M. E. M. Jorge · M. I. da Silva Pereira
CCMM, Department of Chemistry and Biochemistry, University of Lisbon, Campo Grande C8,
1749-016 Lisbon, Portugal
e-mail: aboavida@fc.ul.pt

K. Lobato
SESUL – Center for Sustainable Energy Systems,
University of Lisbon,
1749-016 Lisbon, Portugal

L. Ciriaco · A. Lopes
Department of Chemistry, UMTP, University of Beira Interior,
6201-001 Covilhã, Portugal

Keywords Metal matrix nanocomposites · Electrodeposition · Thermal treatment · Pharmaceuticals degradation

Introduction

The removal of organic pollutants from wastewater is currently one of the major concerns in environmental control. There is growing interest in the environmental relevance of pharmaceutical drugs in waters [1]. Thousands of tons of drugs are consumed worldwide per year, including a high number of analgesics (e.g., acetominophen, ibuprofen), antibiotics (e.g., amoxicillin), and estrogens, which have been found as pollutants in sewage treatment plant effluents.

To avoid the dangerous accumulation of drugs in the aquatic environment, research efforts are underway to develop more powerful methods than those currently applied in wastewater treatment [2]. Thus, the search for new efficient methods for the degradation of these compounds is a priority. Electrochemical and photoelectrochemical degradation can be suitable and low-cost alternatives to those used presently. The implementation of these methods is closely linked with the development of stable, non-pollutant, cheap and electrocatalytic/photocatalytic electrode materials. In this work, composite electrodes of Ti/Zn-TiO_2 have been prepared to be used in pharmaceutical degradation by photoassisted electrochemical processes. The use of composites electrodes, with a metallic matrix, on the organic pollutant degradation, is still rare, although some studies indicate that the metallic matrix has a positive influence on the photocatalytic activity of the semiconductor [3].

The nanocomposite coatings were prepared by the occlusion electrodeposition method, where high surface area TiO_2 nanoparticles are incorporated within the metal matrix, while simultaneously reduction of the metal ions occurs at the interface electrode solution [4, 5]. This method has been selected for its versatility and simplicity.

With a wide band gap (3.35 eV) [6], ZnO has been used as an environmental photocatalyst for water purification with the aid of artificial light source [7]. Among the techniques used for the oxidation of Zn films, heat treatment seems to be the simplest [8, 9]. Moreover, some reports point to the formation of nanocrystalline ZnO films with higher surface area that is very interesting to a variety of technological applications [10]. Thus, after electrodeposition, the films were heated in air to oxidize Zn metal matrix. After heat treatment, it is expected that the Zn matrix will be converted to ZnO. We successfully used this strategy to prepare Ti/ZnO-TiO_2 photoelectrodes for the degradation of the AO7 dye in aqueous solution [11]. Other published studies reveal the gas-phase photocatalytic activity of Zn-TiO_2 prepared on steel substrates [12, 13], and clearly indicate that further research is needed to find out the full potential of photoelectroactive composite electrodes prepared by electrochemical deposition methods.

The goal of this work consisted in the preparation of photoelectroactive Ti/Zn-TiO_2 thin films that could be used for the degradation of pharmaceuticals in aqueous solutions. It is expected that this material after annealing acts as a good candidate for the photoelectrochemical degradation of organic compounds due to the conversion of Zn to ZnO and to the substantial increase in active area. Ibu was chosen as "model" pharmaceutical as it is widely used for its analgesic, anti-inflammatory and antipyretic properties and because it belongs to the group of propionic acid derivatives [14, 15]. Ibuprofen degradation has been studied by different methods: photolysis with UV radiation and UV/H_2O_2 [16, 17], photo-Fenton [18], photocatalytic process, with TiO_2, [19, 20], and electrochemical methods — namely, electro-Fenton, UVA photoelectro-Fenton and solar photoelectro-Fenton — using BDD or Pt anodes [21], most of them with very good degradation of the parent compound. BDD electrodes are well recognized by their excellent proprieties (low background current, wide working potential window) and their main disadvantage (its high price). Other materials like Ti/Pt/PbO_2 and Ti/SnO_2-Sb_2O_4 oxide anodes were also used in the electro-oxidation of Ibuprofen, with very high degree of mineralization after 24 h of degradation [22, 23]. Comparatively to the published studies, the materials prepared in this study are cheap, photoactive with high surface area leading to a significant photoconversion efficiency that makes them adequate photoanodes for the degradation of Ibu.

Experimental

Nanocomposite electrodeposition and thermal treatment

The electroplating bath was a mixture of 0.10 mol dm^{-3} $ZnSO_4 \cdot 7H_2O$ (Sigma-Aldrich; 99.0%), 0.20 mol dm^{-3} $MgSO_4$ (Sigma-Aldrich; ≥99.0%) and 0.15 mol dm^{-3} H_3BO_3 (Panreac, 99.8%). For the nanocomposite films preparation, 10 gdm^{-3} TiO_2 (Aeroxide® TiO_2 P25, particle size approx. 25 nm, with chemical composition of 80% anatase and 20% rutile) were added to the solution. The bath pH was adjusted to 4 by adding a H_2SO_4 diluted solution. The solutions were made daily without further purification, followed by deaeration with nitrogen before and during the electrodeposition.

A glass cell with two compartments was used, with a Zn plate as a sacrificial counter-electrode and a commercial Ag/AgCl as reference. The working electrode was a Ti disc with 0.8 cm^2 area (Goodfellow). The Ti disc was etched with HF 40%, polished with 0.05-μm silica powder (Buehler) and ultrasonically cleaned for 10 min with Millipore Milli-Q ultrapure water (18 MΩ cm).

The Ti/Zn and Ti/Zn-TiO_2 nanocomposite films were prepared by pulsed-reverse current technique. The values of the pulse-plating parameters, average current densities, duty cycle and frequency are shown in Table 1, where i_c and i_a represent the cathodic and anodic density pulse currents, t_c and t_a the cathodic and anodic pulse durations, i_m the average density current, γ the duty cycle and f the pulse frequency.

The electrochemical depositions were carried out using an EG&G Princeton Applied Research potentiostat/galvanostat, Model PAR 263.

The deposition was performed under magnetic stirring (150 rpm) at room temperature for 100 min in order to obtain an average charge value of 30 C. When finished, the electrode was removed from the cell, rinsed with Millipore Milli-Q ultra pure water and dried under nitrogen atmosphere for 5–10 min at room temperature. The estimated theoretical thickness of the electrodeposits was 18 μm. In a previous work it has been demonstrated that the theoretical thickness value match well with the experimental values

Table 1 Electrodeposition parameters

i_c / mA cm^{-2}	i_a (mA cm^{-2})	t_c (ms)	t_a (ms)	i_m (mA cm^{-2})	γ (%)	f (Hz)
−19	19	16	8	6	67	42

obtained from cross-section SEM images [24], which points to high current efficiencies [5].

The as-deposited Ti/Zn and Ti/Zn-TiO_2 films were annealed in air at 450 °C, using a heating rate of 5 °C min^{-1}, held for 6 h, and then cooled to room temperature. A conventional Naberterm furnace controlled by Logotherm Program Controller S19 was used.

Films characterization

The structural characterization of the electrodeposits was carried out by X-ray diffraction (XRD), on a Philips Analytical PW 3050/60 X'Pert PRO ($\theta/2\theta$) equipped with X'Celerator detector and with automatic data acquisition (X'Pert Data Collector (v2.0b) software), using a monochromatized Cu Kα radiation as the incident beam, operating at 40 kV–30 mA. XRD diffraction patterns were obtained by continuous scanning in a 2θ range of 20–90° with a 2θ-step size of 0.02° and a scan step time of 10 s. The average films crystallite size were calculated from the X-ray line broadening according to the Scherrer equation: $D = 0.9\lambda/B\cos\theta$, where λ is the wavelength of the Cu Kα radiation, B ($B^2 = B_M^2 - B_S^2$) is the difference in the full-width at half-maximum (FWHM) of XRD peaks for the specimen (B_M) and standard sample (B_S) (in this study, silicon standard was used), and θ is the Bragg diffraction angle of the line [25]. The peak broadening analysis was applied to Zn (101) reflection.

The films morphology and elemental composition were investigated by field emission scanning electron microscopy (FEG-SEM JEOL 7001 F) coupled with energy-dispersive spectroscopy (EDS), with an electron beam voltage of 25 kV.

Photoelectrochemical tests

The photoelectroactivity of the annealed Ti/Zn-TiO_2 electrodes, with a geometrical area of 0.8 cm^2, was evaluated by linear voltammetry in 0.035 mol dm^{-3} Na_2SO_4 (Merck; 99.0%) aqueous solution under illumination at λ=365 nm chopped at 0.1 Hz of frequency, using Ag/AgCl and platinum as reference and counter-electrodes, respectively. For comparison, measurements with annealed Ti/Zn electrodes were also performed.

The Ibuprofen degradation tests were performed in 0.035 mol dm^{-3} Na_2SO_4 aqueous solution (pH 6.2) as supporting electrolyte with 50 mg dm^{-3} sodium 2-(4-isobutylphenyl) propionate, known as Ibuprofen with a purity of 99.9% (Sigma-Aldrich; used as purchased without further purification). The working electrode was illuminated by means of a light source (Lot Oriel Apex housing with a 200-W EmArc™ lamp) through a quartz window. The distance of the working electrode was adjusted so that the whole active area of the working electrode was illuminated. The resulting light intensity approximated 100 mW cm^{-2}. The tests were carried out at 1.0 V vs. Ag/AgCl under stirring for 3 h. The solution volume was 100 ml. The solution was stirred in the dark for 30 min, in order to achieve the adsorption equilibrium of the organic molecules on the catalyst surface.

The photoelectrodegradation process was followed by UV–Visible spectroscopy, from 200 to 600 nm by a UNICAM He ion UV–Vis spectrophotometer. The Ibu concentration was determined by monitoring the absorbance at λ= 220 nm. Measurements of chemical oxygen demand (COD), following the titrimetric method, according to standard methods [26], and total organic carbon (TOC), using a Shimadzu TOC-VCPH/CPN apparatus were also performed. The Ibu degradation was confirmed by HPLC (Agilent 1100 Series system) with a Tracer excel 120 ODS-A column (150×4.0 mm, 5 μm) at 25 °C. The mobile phase was 10% water/90% methanol and the flow rate 1.0 ml min^{-1}. The detection wavelength was 220 nm.

Results and discussion

Thermal treatment of the nanocomposite electrodeposits

Figure 1a shows the XRD diffraction patterns obtained for the as-deposited and heated Ti/Zn-TiO_2 films. All reflections of the as-deposited Ti/Zn-TiO_2 have a good match with the crystalline Zn phase (JCPDS 4-831). Between 24° and 28° 2θ (inset of Fig. 1a), small peaks are observed that were attributed to the TiO_2 particles (JCPDS 21-1272 for anatase and 21-1276 for rutile). For comparison the XRD pattern of the Ti/Zn electrodeposits is presented in Fig. 1b. As expected, the only phase detected, beyond the substrate, was the Zn. The (101) reflection of Zn phase is the most intense on both samples, and the (002) diffraction line has a higher intensity for the Ti/Zn-TiO_2 than on Ti/Zn electrodeposits, which is in accordance with our previous work [27]. Values of 60 and 90 nm for the Zn crystallite size were estimated by Scherrer equation, for the Ti/Zn-TiO_2 and Ti/Zn films, respectively.

After the thermal treatment, the starting material, Zn, is transformed into wurtzite-structured ZnO (JCPDS 36-1451), as shown in Fig. 1. The other diffraction peaks observed may be attributed to phases of the Ti–Zn system. In particular, the $TiZn_3$ phase (JCPDS 7-98) was identified as one of the constituents of the film [28]. It should be highlighted that the diffraction peaks attributed to this phase are the most intense in the Ti/Zn sample after annealing (Fig. 1b). In addition, on this particular sample, the intensity of the ZnO diffraction peaks is very weak comparatively to those of $TiZn_3$. The ratio of the most intense peaks of the ZnO and

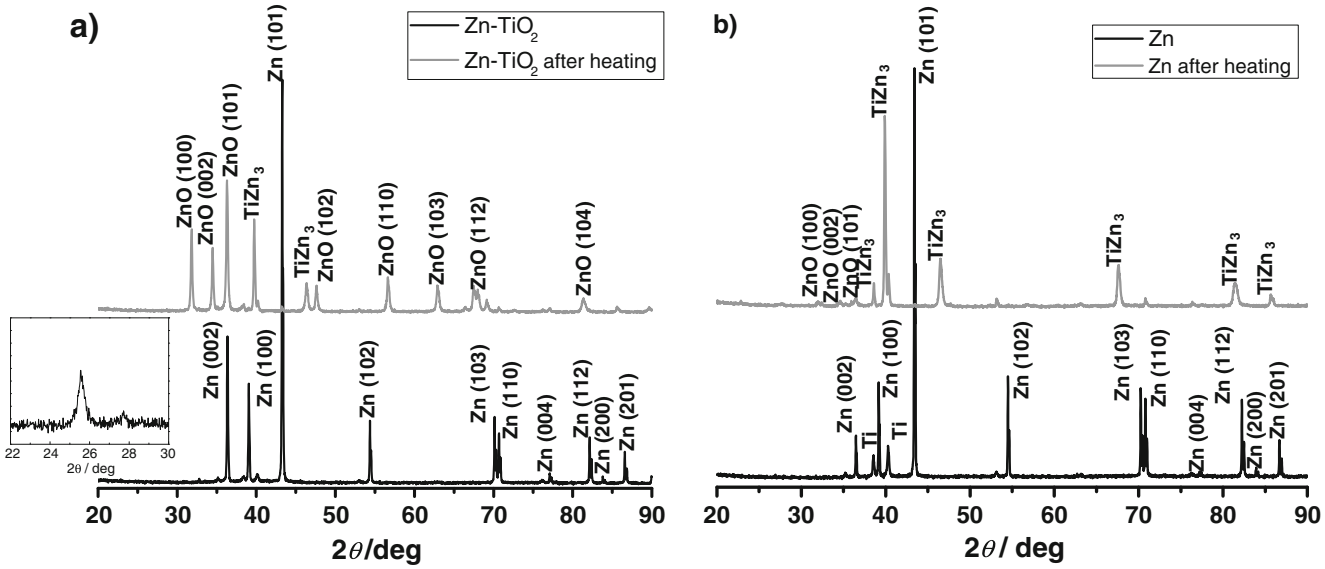

Fig. 1 XRD diffraction patterns of Zn-TiO_2 (**a**) and Zn (**b**) films before and after heat treatment

$TiZn_3$ phases are 1.44 and 0.04 for the annealed samples Ti/Zn-TiO_2 and Ti/Zn, respectively. This result indicates that the conversion of Zn to ZnO was more successful for the Ti/Zn-TiO_2 samples. The success of this conversion should be attributed to the thermal oxidation temperature, Zn phase structural organization and crystallite size and in addition, to the presence of the TiO_2 nanoparticles. The standard Gibbs free energy of formation for ZnO and $TiZn_3$ is, respectively, −556.4 and −68.5 kJ mol^{-1} at 450 °C assuming Eqs. 1 and 2 [29, 30].

$$2Zn + O_2 \rightleftarrows 2ZnO \quad \Delta G = -701 + 0.200T \tag{1}$$

$$Ti + 3Zn \rightleftarrows TiZn_3 \quad \Delta G = -108 + 0.055T \tag{2}$$

where $\Delta G°$ is the standard Gibbs free energy of formation and T is the absolute temperature (in K). Although the formation of ZnO is thermodynamically more favourable, it seems that the kinetics parameters, which are intensely affected by the Zn crystallite size and film surface area, strongly control the Zn to ZnO conversion. According to the XRD results, this conversion is easier for low Zn crystallite size films. Similar behaviour has been found when other metallic substrates such as iron, steel and copper were used on the Zn-TiO_2 films preparation [31].

The ZnO cell parameters are very similar for the two samples studied and concordant to the published results,

Table 2 Cell parameters of ZnO phase present on the annealed Ti/Zn and Ti/Zn-TiO_2 samples

Sample	a / Å	c (Å)	V (Å^3)
Ti/Zn-TiO_2 annealed	3.2466±0.0003	5.2008±0.0005	47.48±0.01
Ti/Zn annealed	3.233±0.003	5.185±0.004	46.9±0.1
ZnO[24]	3.24	5.19	47.2

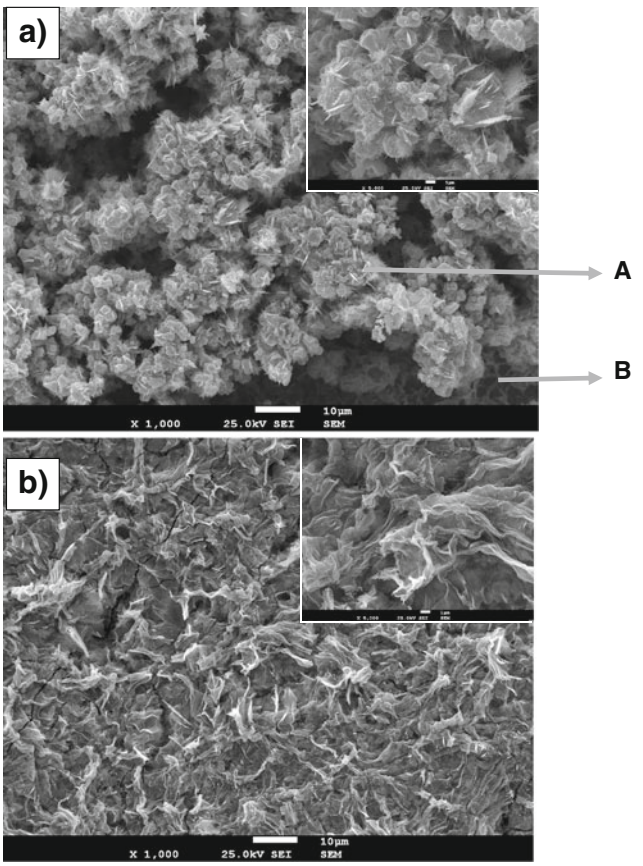

Fig. 2 FEG-SEM images of Zn-TiO_2 (**a**) and Zn (**b**) films after heat treatment

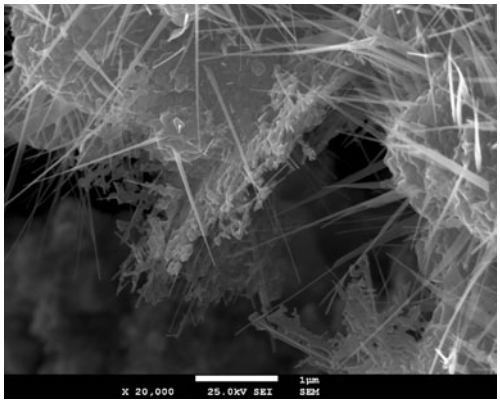

Fig. 3 Details of needled morphology

a=3.24 Å and c=5.19 Å [32], as Table 2 shows. There are no significant variations in the calculated structural parameters, and only a slightly decrease in the calculated error for the Ti/ZnO-TiO_2 sample is seen. This may be associated with the better definition of the diffraction peaks due to the higher amount of ZnO phase formed.

The surface morphology of the annealed Ti/Zn-TiO_2 electrodes (Fig. 2a) is very porous and comprises a three-layered structure of scattered petal like particles, located on the region near the substrate, and porous microdiscs clusters with needled shaped nanograins composed by Zn and O as identified by EDS. These needles measure about ~2 μm in length with a diameter of 50–60 nm measured at the base and are randomly grown in different directions with their base attached to the porous discs clusters (Fig. 3). These results are similar to those reported by Deguchi et al. [13], who assume that TiO_2 particles incorporated in Zn matrix can act as seeds for the ZnO whiskers growth.

In the absence of TiO_2 particles (Fig. 2b), the Ti/Zn annealed films are more compact and the needled shaped grains are not present. The difference observed for the two deposits could be related to the morphological characteristics of the as-deposited Zn-TiO_2 and Zn films (Fig. 4a and b, respectively). Due to the particles' incorporation, the zinc grains in the nanocomposite films became smaller with more grain frontiers and, consequently, the Zn-TiO_2 surface is rougher and more irregular than the Zn electrodeposits.

Table 3 presents the average EDS results obtained, after heat treatment, for the samples Ti/Zn and Ti/Zn-TiO_2: zones A and B as indicated in Fig. 2a. The composition analysis of zone A revealed that the atomic ratio of zinc to oxygen is approximately 1, and a very low amount of Ti is detected, which indicates that in this zone the film is mostly composed by ZnO. The composition of zone B is quite similar to the composition of samples Ti/ZnO, which points to a heterogeneous composition of the Ti/Zn-TiO_2 samples after annealing. These results are in accordance with the XRD data.

Distinct crystal growth mechanisms have been considered in the literature to interpret the growth mechanism of the different ZnO morphologies observed, namely, the one-dimensional (1D) nanostructures [10, 33, 34]. Unanimously, these studies mention that the Zn crystal orientation is crucial to the oxidation process [10]. According to the literature, the formation of porous nanosheets can be explained by a vapour–solid mechanism that consists of two stages: nucleation and growth [35, 36]. It is expected that at the annealing temperature Zn sublimation occurs, with the formation of Zn vapour aero-spheres located near the surface [37]. Due to the Zn different atomic packing of the crystallographic planes, with the (002) plane being the most packed, the sublimation will occur with different rates. The vapour reacts with oxygen, forming ZnO nuclei. As consequence of growth of these nuclei, a redeposition occurs with the formation of open porous structures. At this temperature, the formation of nanorods at the edge of porous structures is also possible [34, 35]. In other words, it is supposed that the thin oxide film formed during the thermal treatment on the surface of the zinc particles in air played an important role in the generation of the ZnO nanorods. The oxidation of Zn will take place upon grain boundaries or cleavages of the oxide layer formed naturally on the surface of zinc particles, which results in the formation of ZnO nanorods. This growth along one direction is very sensitive to the temperature: at higher temperatures, diffusion of Zn^{2+}

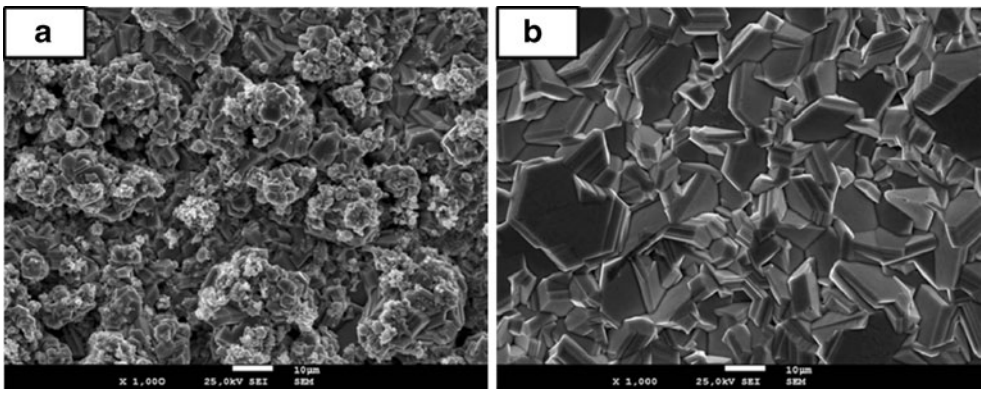

Fig. 4 FEG-SEM images of Zn-TiO_2 (**a**) and Zn (**b**) as-deposited films

Table 3 EDS average results obtained, after heat treatment, for Ti/Zn and Ti/Zn-TiO_2 samples

Elements (at.%)	Samples		
	Ti/Zn-TiO_2 annealed		Ti/Zn annealed
	Zone A[a]	Zone B[a]	
O	48.68±0.90	46.29±5.29	51.22±4.02
Ti	1.71±0.03	17.02±6.48	13.35±2.45
Zn	49.61±0.92	36.70±1.29	35.38±1.51
Zn/O ratio	1.02	0.79	0.69
Ti/Zn ratio	0.03	0.46	0.38

[a] As identified in Fig. 2a

ions will be much faster [34]. With time, the amount of ions reaching the 1D tip decreases resulting in the formation of nanoneedles [10]. Liu et al. [36] reported that ZnO nanowires preferably grow from porous Zn films than from compact ones. For porous Zn films with small crystallites it is easier to form Zn vapour and consequently microporous disc clusters plus nanoneedles. At the nanocomposite film regions, where the Zn grains have higher dimensions and other preferable orientation, this process is more difficult to occur and this type of morphology is not seen. This is comparable to what happens with the Zn electrodeposits during the thermal treatment, where the main diffusion process is diffusion of Zn through the titanium interface, resulting on the formation of TiZn intermetallics.

Photoelectrochemical tests

Photovoltammograms of annealed Ti/Zn-TiO_2, Ti/Zn and Ti electrodes in 0.035 mol dm^{-3} Na_2SO_4 aqueous solution were recorded under illumination at λ=365 nm (Fig. 5). A positive photocurrent is observed for all samples, indicating

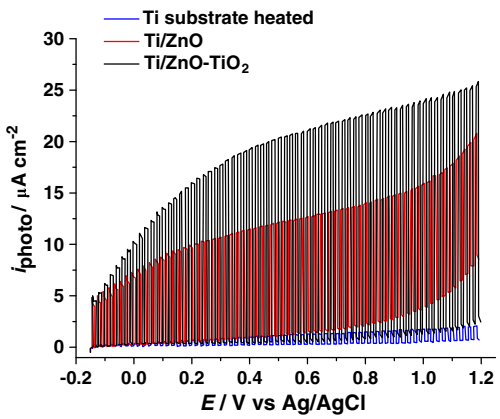

Fig. 5 Photovoltammograms of annealed Ti/Zn-TiO_2 and Ti/Zn electrodes in 0.035 mol dm^{-3} Na_2SO_4 aqueous solution (pH 6.2) under λ= 365 nm irradiation chopped at 0.1 Hz of frequency. Sweep rate 2 mV s^{-1}

their n-type behaviour. As shown, the photocurrent is strongly dependent on the potential value: increasing with the applied potential and reaching a stable value at 0.4 V vs. Ag/AgCl. It is clearly seen that for all the potential values swept, the photocurrent generated by the annealed Ti/Zn-TiO_2 electrode is higher than for the heat-treated Zn electrode, and in the case of the Ti thermal treated, the photocurrent is negligible. The marked enhancement of the activity may arise from the increase in the photoactive surface area caused by the growth of the ZnO nanoneedles as well as to the presence of

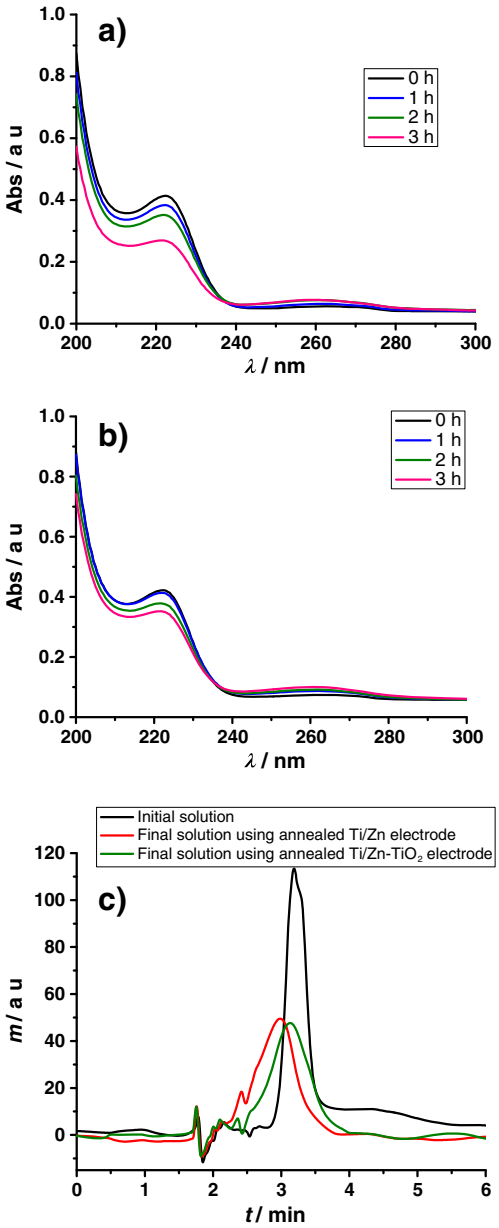

Fig. 6 UV spectra for samples collected during the photoelectrolysis performed in 0.035 mol dm^{-3} Na_2SO_4 aqueous solution (pH 6.2) with 50 mg dm^{-3} Ibuprofen under UV-enhanced white light irradiation (100 mW cm^{-2}) and 1 V vs. Ag/AgCl with Ti/Zn-TiO_2 (**a**) and Ti/Zn (**b**) annealed anodes (0.8 cm^2). **c** HPLC spectra

the TiO_2 nanoparticles. The high surface area may increase light trapping and consequently photon absorption leading to an increasing electron–hole pair generation, and/or expose a greater number of holes to the oxide surface, allowing the reduction of the species within the electrolyte. The photocurrent increase with applied bias, indicates a significant and tuneable electric field (band bending is present) leading to an efficient charge separation. This leads to a greater number of holes at the oxide surface to react with H_2O/OH^- to give rise to $OH^{\bullet}$ radicals, which in turn react strongly with organic molecules [38]. According to the literature, the semiconductors ZnO and TiO_2 have similar band gap values, and the ZnO conduction band is more negative than TiO_2 [39, 40], which could be beneficial to minimize the electron–hole recombination process and consequently maximize the photocurrent generation on the Ti/ZnO-TiO_2 electrodes.

Figure 5 shows that the dark current is higher on the annealed Ti/Zn than on the annealed Ti/Zn-TiO_2 electrodes. As noted before, this sample contains the highest $TiZn_3$ phase amount. This intermetallic material could be oxidized or participate on anodic processes involving the solution, namely, the water oxidation, which might be responsible for the observed trend. Other process that could not be discarded is the electrochemical oxidation of Ibu [22].

UV–Vis spectroscopy (Fig. 6a and b) was used to monitor the Ibu photoelectrodegradation performed at 1.0 V vs. Ag/AgCl. An intense peak characteristic of the Ibu is observed at λ=220 nm, followed by a weak band at 264 nm. A decrease in peak intensity occurs with the photoelectrolysis time and, simultaneously, the weak band at 264 nm increases and shifts to approximately 260 nm. These results, more evident for the Ti/ZnO-TiO_2 photoelectrodes, indicate that the concentration of the Ibu decreases in solution and

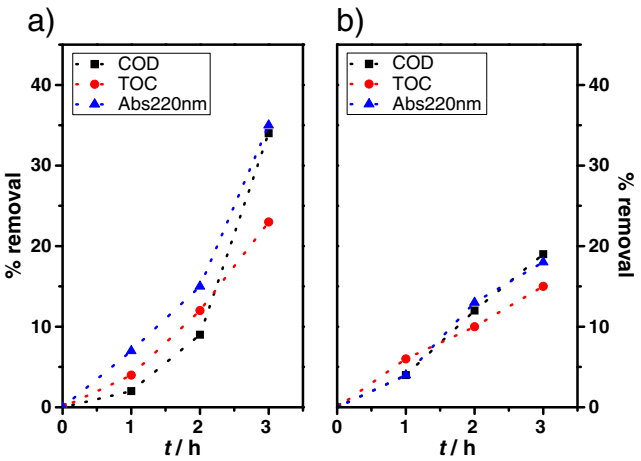

Fig. 7 Removals of COD, TOC and Abs at 220 nm for samples collected during the Ibu photoelectrodegradation in 0.035 mol dm^{-3} Na_2SO_4 aqueous solution (initial pH 6.2) with 50 mg dm^{-3} Ibuprofen under UV-enhanced white light irradiation (100 mW cm^{-2}) at 1 V vs. Ag/AgCl with Ti/Zn-TiO_2 (**a**) and Ti/Zn (**b**) annealed anodes (0.8 cm^2)

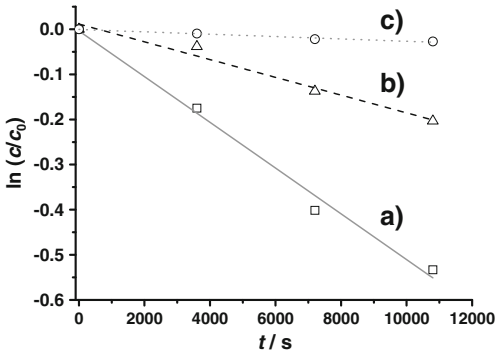

Fig. 8 Kinetic analysis considering a pseudo-first-order (ln (c/c_0) vs. t) for ibuprofen degradation by photoelectrochemical process using Ti/Zn-TiO_2 (**a**) and Ti/Zn (**b**) annealed anodes, and by electrochemical process using annealed Ti/Zn-TiO_2 (**c**)

decomposition products are formed, in accordance with the behaviour already published in the literature [22, 41]. It should be noted that the as-prepared Ti/Zn-TiO_2 electrodes were tested as anodes for the Ibuprofen photoelectrochemical degradation but the % removal was very low.

In Fig. 6b, the band observed at 260 nm may be associated with the formation of new C–O bonds, promoted by the attack of strong oxidizing species, such as hydroxyl radicals [41]. In particular, the attack to the tertiary carbon of the isobutyl group by hydroxyl radicals, leading to a posterior formation of double conjugated bonds, to give 2-[4-(carboxycarbonyl)phenyl] propanoic acid, is very probable [22]. This type of mechanism was observed by Quintana et al. [42] during the degradation of ketoprofen. The formation of that compound must be followed by the opening of the aromatic ring, as indicated by the decrease in the band at 220 nm, where the aromatic rings usually absorb.

The HPLC spectra (Fig. 6c) clearly show a decrease in the Ibu amount present in the solutions after the photoelectrochemical degradation process. For the Ti/ZnO-TiO_2 photoelectrodes, the very similar removals of COD, TOC and absorbance observed for the first 2 h of photoelectrolysis

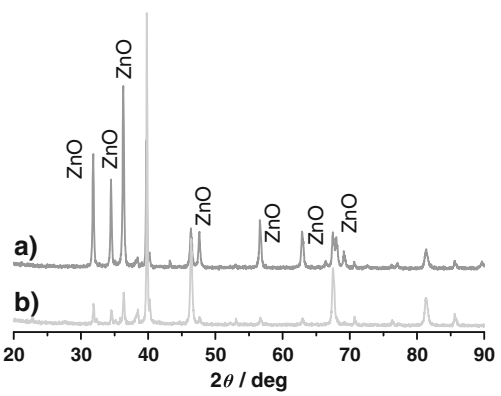

Fig. 9 XRD diffraction patterns of the annealed Ti/Zn-TiO_2 films before (**a**) and after the Ibu degradation (**b**)

denote that the oxidation happens almost simultaneously with the elimination of organic carbon from the solution, corroborating a fast mineralization mechanism (Fig. 7).

COD and TOC data show removals of 34% and 23%, respectively, after 3 h of degradation. These results point to Ibuprofen being photoelectrochemically degraded. The values of COD, TOC and absorbance are lower when annealed Ti/ZnO is used, as expected. In a future work, we are planning to identify the intermediate and final products in order to suggest a possible mechanism of Ibu photoelectrochemical degradation.

Assuming that Ibu degradation follows a pseudo-first order kinetic process [21, 43], the graphical representation of ln (c/c_0) vs. t was done (Fig. 8), where c_0 is the initial concentration of Ibu, and c is the concentration of Ibu after t degradation period. The apparent first-order rate constant has a value of 5.07×10^{-5} s^{-1} (R^2=0.986) and 1.97×10^{-5} s^{-1} (R^2=0.963) for annealed Ti/Zn-TiO_2 and Ti/Zn electrodes, respectively. This tendency confirms the expected increased production of $OH^{\bullet}$ radicals when Ti/ZnO-TiO_2 photoelectrodes are used. Also, from this graphic, it could be assumed that no electrochemical oxidation contributes to the Ibu degradation, as evidenced by the almost constant Ibu concentration during the electrochemical process at 1.0 V vs. Ag/AgCl without illumination.

Figure 9 shows the XRD patterns of the Ti/ZnO-TiO_2 electrodes after the photoelectrochemical tests. As can be seen, the ZnO reflections have a significant decrease which points out to a deficient stability of this phase. This should be associated to a dissolution process stimulated by the light irradiation. Other authors indicated that the phenomenon of photo-dissolution of ZnO thin films can occur [44–46]. Ongoing work is being undertaken in order to minimize this problem in order to allow the ready usage of these materials in water treatment applications.

Conclusions

Photoactive annealed Ti/Zn-TiO_2 electrodes were successfully prepared and used for the first time on the photoelectrochemical degradation of Ibuprofen. The XRD analysis of the deposits points to the metal matrix modification from Zn to ZnO. In addition, the SEM results indicate that the films have an elevated area with a rich morphology, namely, the appearance of ZnO needle-shaped grains.

The photoassisted electrochemical degradation of the Ibuprofen was observed by UV–Vis spectrometry, HPLC, COD and TOC. The data show that Ibuprofen was efficiently degraded. Absorbance at 220 nm, COD and TOC removals of 35%, 34% and 23%, respectively, were obtained for the initial 3 h of photoelectrolysis using annealed Ti/Zn-TiO_2 electrodes. The apparent first-order rate constant for Ibu degradation has a value of 5.07×10^{-5} s^{-1} (R^2=0.986). These promising results reveal that this nanocomposite material has a huge potential to be applied as photoelectrocatalyst.

Acknowledgements The authors acknowledge financial support from Fundação para a Ciência e Tecnologia (Portugal), under research project PTDC/CTM/64856/2006. The authors acknowledge to Professor J.M. Nogueira (University of Lisbon) for the HPLC analyses.

References

1. Buser HR, Poiger T, Müller MD (1999) Occurrence and Environmental Behavior of the Chiral Pharmaceutical Drug Ibuprofen in Surface Waters and in Wastewater. Environ Sci Techno 33:2529–2535
2. Skoumal M, Cabot PL, Centellas F, Arias C, Rodriguez RM, Garrido JA, Brillas E (2006) Mineralization of paracetamol by ozonation catalyzed with Fe^{2+}, Cu^{2+} and UVA light. Appl Cat B: Environ 66:228–240
3. Zhou M, Tacconi NR de, Rajeshwar K (1997) Preparation and characterization of nanocrystalline composite (nanocomposite) films of titanium dioxide and nickel by occlusion electrodeposition. Electroanal Chem 421:111–120
4. Gomes A, Pereira MI da Silva, Mendonça MH, Costa FM (2005) Zn–TiO_2 composite films prepared by pulsed electrodeposition. J Solid State Electrochem 9: 190–196
5. Frade T, Bouzon V, Gomes A, Pereira MI da Silva (2010) Pulsed-reverse current electrodeposition of Zn and Zn-TiO_2 nanocomposite films. Surf Coat Tech 204:3592-3598
6. Bard AJ, Stratmann, Licht S (eds) (2002) Encyclopedia of Electrochemistry, Vol. 6, Semiconductor Electrodes and Photoelectrochemistry, Wiley-VCH, Weinheim
7. Fouad OA, Ismail AA, Zaki ZI, Mohamed RM (2006) Zinc oxide thin films prepared by thermal evaporation deposition and its photocatalytic activity. Appl Cat B: Environ 62:144–149
8. Chen SJ, Liu YC, Ma JG, Zhao DX, Zhi ZZ, Lu YM, Zhang JY, Shen DZ, Fan XW (2002) High-quality ZnO thin films prepared by two-step thermal oxidation of the metallic Zn. J Crystal Growth 240:467–472
9. Alivov YI, Chernykh AV, Chukichev MV, Korotkov RY (2005) Thin polycrystalline zinc oxide films obtained by oxidation of metallic zinc films. Thin Solid Films 473:241–246
10. Yuvaraj D, Rao KN (2009) Selective growth of ZnO nanoneedles by thermal oxidation of Zn microstructures. Mater Sci Eng B 164:195–199
11. Frade T, Gomes A, Pereira MI da Silva, Lopes A, Ciríaco L (2011) Fotoelectrodegradação do Corante AO7 utilizando filmes de nanocompósitos de ZnO-TiO_2 (abstract in english). Química Nova (in press)
12. Ito S, Deguchi T, Imai K, Iwasaki M, Tada H (1999) Preparation of Highly Photocatalytic Nanocomposite Films Consisting of TiO_2 Particles and Zn Electrodeposited on Steel. Electrochem Solid State Lett 2:440–442
13. Deguchi T, Imai K, Iwasaki M, Tada H, Ito S (2000) Photocatalytically Highly Active Nanocomposite Films Consisting of TiO_2 Particles and ZnO Whiskers Formed on Steel Plates. J Electrochem Soc 147:2263–2267
14. Madhavan J, Grieser F, Ashokkumar M (2010) Combined advanced oxidation processes for the synergistic degradation of ibuprofen in aqueous environments. J Hazard Mater 178:202–208

15. Zhao X, Qu J, Liu H, Qiang Z, Liu R, Hu C (2009) Photoelectrochemical degradation of antiinflammatory pharmaceuticals at Bi_2MoO_6–boron-doped diamond hybrid electrode under visible light irradiation. Appl Cat B: Environ 91:539–545
16. Yuan F, Hu C, Hu X, Qu J, Yang M (2009) Degradation of selected pharmaceuticals in aqueous solution with UV and UV/H_2O_2. Water Res 43:1766–1774
17. Matamoros V, Duhec A, Albaigés J, Bayona J (2009) Photodegradationof Carbamazepine, Ibuprofen, Ketoprofen and 17α-Ethinylestradiol in Fresh and Seawater. Water Air Soil Poll 196:161–168
18. Méndez-Arriaga F, Esplugas S, Giménez J (2010) Degradation of the emerging contaminant ibuprofen in water by photo-Fenton. Water Res 44:589–595
19. Méndez-Arriaga F, Esplugas S, Giménez J (2008) Photocatalytic degradation of non-steroidal anti-inflammatory drugs with TiO_2 and simulated solar irradiation. Water Res 42:585–594
20. Achilleos A, Hapeshi E, Xekoukoulotakis N P, Mantzavinos D, Fatta-Kassinos D (2010) UV-A and Solar Photodegradation of Ibuprofen and Carbamazepine Catalyzed by TiO_2. Separ Sci Technol 45:1564–1570
21. Skoumal M, Rodriguez RM, Cabot PL, Centellas F, Garrido JA, Arias C, Brillas E (2009) Electro-Fenton, UVA photoelectro-Fenton and solar photoelectro-Fenton degradation of the drug ibuprofen in acid aqueous medium using platinum and boron-doped diamond anodes. Electrochim Acta 54:2077–2085
22. Ciríaco L, Anjo C, Correia J, Pacheco MJ, Lopes A (2009) Electrochemical degradation of Ibuprofen on Ti/Pt/PbO_2 and Si/BDD electrodes. Electrochim Acta 54:1464–1472
23. Ciríaco L, Santos D, Pacheco MJ, Lopes A (2011) Anodic oxidation of organic pollutants on a Ti/SnO_2–Sb_2O_4 anode. J Appl Electrochem 41:577–587
24. Alberts D, Fernández B, Frade T, Gomes A, Pereira MI da Silva, Pereiro R, Sanz-Medel A (2011) Depth profile characterization of Zn–TiO_2 nanocomposite films by pulsed radiofrequency glow discharge-optical emission spectrometry. Talanta 84:572–578
25. Cullity BD (1978) Elements of X-ray Diffraction, 2nd ed., Addison-Wesley, Reading, MA
26. Eaton A, Clesceri L, Greenberg A (2005) Standard Methods for Examination of Water and Wastewater, 21st ed., American Public Health Association, Washington
27. Fustes J, Gomes A, Pereira MI da Silva (2008) Electrodeposition of Zn–TiO_2 nanocomposite films-effect of bath composition. J Solid State Electrochem 12:1435-1443
28. Tang X, Yin F, Wang X, Wang J, Su X, Tang N-Y (2007) The 450 °C Isothermal Section of the Zn-Fe-Ti System. J Phase Equilib Diffus 28:355–361
29. Xu CH, Zhu ZB, Li GL, Xu WR, Huang HX (2010) Growth of ZnO nanostructure on $Cu_{0.62}Zn_{0.38}$ brass foils by thermal oxidation. Mater Chem Phys 124:252–256
30. Doi K, Ono S, Ohtani H, Hasebe M (2006) Thermodynamic study of the phase equilibria in the Sn−Ti−Zn ternary system. J Phase Equilib Diffus 27:63-74
31. Frade T (2010) Preparação e Caracterização de Nanomateriais para Serem Utilizados como Fotocatalizadores no Tratamento de Águas Contaminadas por Medicamentos (in portuguese), Dissertation of Master's Degree in Chemistry, Faculty of Science of University of Lisbon, Lisbon
32. Zhang X G (1996) Corrosion and Electrochemistry of Zinc, Plenum Press, New York
33. Park JY, Lee DJ, Kim SS (2005) Size control of ZnO nanorod arrays grown by metalorganic chemical vapour deposition. Nanotechnology 16:2044–2047
34. Yu W, Pan C (2009) Low temperature thermal oxidation synthesis of ZnO nanoneedles and the growth mechanism. Mater Chem Phys 115:74–79
35. Tan WK, Razak KA, Ibrahim K, Lockman Z (2011) Oxidation of etched Zn foil for the formation of ZnO nanostructure. J Alloys Comp 509:6806–6811
36. Liu ZW, Yeo SW, Ong CK (2007) An alternative approach to *in situ* synthesize single crystalline ZnO nanowires by oxidizing granular zinc film. J Mater Sci 42:6489–6493
37. Gao PX, Lao CS, Ding Y, Wang ZL (2006) Metal/Semiconductor Core/Shell Nanodisks and Nanotubes. Adv Funct Mater 16:53–62
38. ZanoniM VB, Sene JJ, Anderson MA (2003) Photoelectrocatalytic degradation of Remazol Brilliant Orange 3R on titanium dioxide thin-film electrodes. J Photochem Photobiol A: Chem 157:55–63
39. Lei Y, Zhao G, Liu M, Zhang Z, Tong X, Cao T (2009) Fabrication, Characterization, and Photoelectrocatalytic Application of ZnO Nanorods Grafted on Vertically Aligned TiO_2 Nanotubes. J Phys Chem C 113:19067–19076
40. Zhang Z, Yuan Y, Liang L, Cheng Y, Shi G, Jin L (2008) Preparation and photoelectrocatalytic activity of ZnO nanorods embedded in highly ordered TiO_2 nanotube arrays electrode for azo dye degradation. J Hazard Mater 158:517–522
41. Brillas E, Sirés I, Arias C, Cabot PL, Centellas F, Rodríguez RM, Garrido JA (2005) Mineralization of paracetamol in aqueous medium by anodic oxidation with a boron-doped diamond electrode. Chemosphere 58:399–406
42. Quintana JB, Weiss S, Reemtsma T, (2005) Pathways and metabolites of microbial degradation of selected acidic pharmaceutical and their occurrence in municipal wastewater treated by a membrane bioreactor. Water Res 39:2654–2664
43. Hu A, Zhang X, Oakes KD, Peng P, Zhou YN, Servos MR (2011) Hydrothermal growth of free standing TiO_2 nanowire membranes for photocatalytic degradation of pharmaceuticals. J Hazard Mater 189:278–285
44. Han J, Qiu W, Gao W (2010) Potential dissolution and photodissolution of ZnO thin films. J Hazard Mater 178:115–122
45. Neppolian B, Choi HC, Sakthivel S, Arabindoo B, Murugesan V (2002) Solar/UV-induced photocatalytic degradation of three commercial textile dyes. J Hazard Mater 89:303–317
46. Dijken A van, Janssen AH, Smitsmans MHP, Vanmaekelbergh D, Meijerink A (1998) Size-Selective Photoetching of Nanocrystalline Semiconductor Particles. Chem Mater 10:3513–3522